# The Influence of Optimization Target Selection on the Structure of Arterial Tree Models Generated by Constrained Constructive Optimization

WOLFGANG SCHREINER,* FRIEDERIKE NEUMANN,* MARTIN NEUMANN,‡ ADELHEID END,* SUSANNE M. ROEDLER,§ and SEYEDHOSSEIN AHARINEJAD||

From the *Department of Cardiothoracic Surgery, Working Group for Biomedical Computer Simulation; ‡Institute for Experimental Physics, Division of Computational Physics; §Departments of Cardiology and ||Anatomy, University of Vienna, A-1090 Vienna, Austria

ABSTRACT The computational method of constrained constructive optimization was used to generate complex arterial model trees by optimization with respect to a target function. Changing the target function also changes the tree structure obtained. For a parameterized family of target functions a series of trees was created, showing visually striking differences in structure that can also be quantified by appropriately chosen numerical indexes. Blood transport path length, pressure profile, and an index for relative segment orientation show clear dependencies on the optimization target, and the nature of changes can be explained on theoretical grounds. The main goal was to display, quantify, and explain the structural changes induced by different optimization target functions.

## INTRODUCTION

### *Types of Computer Models for Arterial Trees*

The structure of arterial trees serves the purpose of efficiently carrying blood to all sites of tissue supplied by the respective artery. Since a sufficient supply of blood is of vital importance and at the same time a costly task for the organism, the question of optimality most naturally arises (Thompson, 1952; Cohn, 1955; Zamir, 1976). Real arterial trees have been examined morphometrically regarding diameter shrinkage across bifurcations (Zamir, 1988; Zamir and Sinclair, 1988), segment lengths (Zamir and Chee, 1987), and branching angles (Zamir and Chee, 1986). Theoretical work has demonstrated that certain optimization criteria can be formulated that are physiologically reasonable on the one hand (such as minimum intravasal volume) and also lend themselves for optimizing the geometry of single arte-

Address correspondence to Wolfgang Schreiner, Ph.D., FACA, Department of Medical Informatics, University of Vienna, Institut für Medizinishe Computerwissenschaften, Waehringer Guertel 18-20, A-1090 Wien, Austria.

J. GEN. PHYSIOL. © The Rockefeller University Press · 0022-1295/95/10/583/17 $2.00
Volume 106 October 1995 583–599

rial model bifurcations under given conditions of pressures and flows (Kamiya and Toghawa, 1972; Zamir, 1976; Zamir and Bigelow, 1984).

Parallel to these findings, the computer simulation of blood flow through arterial model trees has been developed. These simulations draw on either of two basic concepts: (*a*) compartmental representations (lumped parameter models) (Sun and Gewirtz, 1988; Bruinsma, Arts, Dankelman, and Spaan, 1988) or (*b*) branching tube models. These tube models either represent a specific and rather small subtree modeled after real anatomical data (Rooz, Wiesner, and Nerem, 1985), or they are constructed from root to terminals according to concepts of self-similarity with (or without) a stochastic component (Dawant, Levin, and Popel, 1985; Levin, Dawant, and Popel, 1986; Pelosi, Saviozzi, Trivella, and L'Abbate, 1987; West and Goldberger, 1987). While anatomical models describe severely pruned trees, fractal models, even when based on correct statistical distributions (from which segment diameters, lengths, and angles are drawn), are likely to produce trees that are not geometrically arrangeable in space (perfusing all sites of tissue without intersection of segments).

### *The Method of Constrained Constructive Optimization*

In the light of the above arguments, the method of constrained constructive optimization (CCO) has been developed. It is a procedure for growing model trees under the guidance of optimization principles as follows: the piece of tissue to be perfused is geometrically represented by a perfusion area, and we assume that the total perfusion flow ($Q_{perf}$) is available from a feeding artery at the pressure $p_{perf}$. The arterial tree model, with the root segment starting at the perimeter of the perfusion area, consists of straight cylindrical tubes and bifurcations, through which the total flow should be distributed over the perfusion area as homogeneously as possible. Each terminal segment is assumed to supply a microcirculatory black box, and it is intended that for each black box the same flow ($Q_{term}$) is available at the same pressure ($p_{term}$). Moreover, and in analogy to real vascular trees (Zamir and Chee, 1986), we require that radii at each bifurcation fulfill a bifurcation constraint in the form of a power law, see Eq. 2 below. It is surprising that all these requirements can simultaneously be fulfilled at all, solely by appropriate scaling of segment radii, and regardless of the particular structure (connective structure, geometrical location of segments) of the tree. This fact, for the proof of which we refer to our technical paper (Schreiner and Buxbaum, 1993), offers the possibility to construct and simultaneously optimize a model tree by adding segment after segment, while the tree in each stage of development fulfills all constraints mentioned above.

We start from a degenerate tree of one segment with its proximal end at the perimeter of the perfusion area and the location of its distal end (perfusion site) being drawn from a pseudo random number sequence (PRNS). With the segment length thus given, the radius is set to yield the suitable resistance for the flow $Q_{term}$ against $p_{term}$ when being perfused with the pressure $p_{perf}$ at its proximal end (Poiseuille's law [Fung, 1984]). Note that in this early stage of the tree, a single segment experiences the whole pressure gradient $p_{perf}$–$p_{term}$. Next, the location of the second perfusion site is chosen, and the new terminal segment is connected to the

first, thereby generating a bifurcation at some arbitrary location along the first segment. In this tree, now consisting of three segments, again radii can be scaled so that all constraints are fulfilled for a total inflow of 2 * $Q_{term}$ and equal flow-splitting into both terminals. Part of the pressure gradient occurs along the root segment between the inlet ($p_{perf}$) and the bifurcation, while the remaining pressure drops along both terminals to reach $p_{term}$ at their distal ends. Note that this can be attained regardless of the precise location of the bifurcation. This fact is exploited to introduce optimization as follows: we adopt a target function, e.g., the total volume of the tree, and compute its value for the current geometry. For a different location of the bifurcation we usually can expect a different value of the target function, since moving the bifurcation requires concomitant changes in radii, so as to maintain the constraints. On this basis, a gradient method (Press, Teukolsky, Vetterling, and Flannery, 1992) can be implemented to achieve a geometric optimization by moving the bifurcation so as to minimize the target function while the connective structure remains unchanged.

For the third and all remaining terminal segments the procedure of segment adding involves not only geometrical but also structural optimization. Upon casting the location for a new perfusion site (via PRNS), the new terminal is tentatively connected to each of the preexisting segments of the tree, one after the other. Each connection is geometrically optimized, the target function recorded and the connection dissolved again (connection search). Finally the new terminal is connected permanently to that segment that provided the optimum connection site in terms of the target function.

This procedure of repeatedly adding segments comprises the construction process within constrained constructive optimization.

Structures obtained by CCO combine the complexity of fractal tree models with a perfect arrangeability in space and optimized functionality. Technical details of CCO have been described in a previous article (Schreiner and Buxbaum, 1993).

### *Previous Results and Scope of Present Study*

CCO models were found to reproduce branching angles (Zamir and Chee, 1986), segment radii (Zamir, 1988; Zamir and Sinclair, 1988), and pressure profiles (Chilian, Layne, Klausner, Eastham, and Marcus, 1989) of real coronary arterial trees to a satisfying extent (Schreiner and Buxbaum, 1993; Schreiner, Neumann, Neumann, Roedler, End, Buxbaum, Müller, and Spieckermann, 1994), which legitimizes their use as a reasonable substrate for computer simulations of blood flow through arterial trees.

However, whenever plunging into optimization, the question of what should be optimized most realistically inevitably arises. Although several possible target functions and their relative merits have been contrasted in theoretical treatments (Sherman, 1981; Lefevre, 1982, 1983), we have (for reasons of clarity) restricted our previous CCO studies to total intravasal volume as target function, which is an arbitrary but reasonable choice out of several possible candidates. In the present work, however, we extend the method of CCO to a class of target functions, to examine the impact of the optimization target on structure. For the sake of clarity we

construct a simple family of target functions $T$ by varying the exponent in the following expression:

$$T = const \cdot \sum_{i=1}^{N_{tot}} l(i)\, r^{\lambda}(i) \rightarrow \text{minimum}, \quad (1)$$

where $N_{tot}$ is the total number of segments in the tree, $i$ is the segment index and $\lambda(i)$ and $r(i)$ are segment length and radius, respectively. Choosing this family allows to tune continuously between target functions via the parameter. The constant factor does not influence optimization and is chosen adequately so as to make $T$ represent the sum of segment lengths, surface, volume et cetera of the tree for the respective values of $\lambda$.

To compare the generated trees and thus evaluate the impact of target functions on structure, we calculate a number of characteristic properties of the tree such as the blood transport path length and the pressure profile. For each of these properties the dependence on the target function parameter can be evaluated.

Besides the fact that CCO trees with different target functions look totally different, the impact of the optimization target on functional properties is thus put on a quantitative basis in the present work.

## SIMULATIONS PERFORMED

### *Parameters and Constraints*

Each CCO run has to be based on a set of boundary conditions (constrained CO) representing reasonable physiologic conditions. As in our previous work (Schreiner and Buxbaum, 1993; Schreiner et al., 1994) we assume that a two-dimensional representation of 100 g of left ventricular myocardial tissue should be supplied. This setting is representative for, e.g., a reference LAD or LCX bed in humans (Netter, 1983). Bearing in mind the general concepts of CCO we now list the settings in detail: (*a*) $N_{term}$ (= 4,000) terminal segments for the binary tree model; (*b*) perfusion pressure $p_{perf}$ = 100 mmHg; (*c*) equal pressures at the distal ends of all terminals ($p_{term}$ = 60 mmHg); (*d*) total perfusion flow $Q_{perf}$ = 500 ml/min, based on the following standardized conditions: (*i*) a fully vasodilated state, which increases flow about fourfold (400 ml/(min ×100 g) (Marzilli, Goldstein, Sabbah, Lee, and Stein, 1979); and (*ii*) furthermore, we assume cardiac arrest, so that in addition to diastole systole also becomes available for perfusion, which increases flow by another 25% (1.25 × 400 ml/min = 500 ml/min); (*e*) equal flows through all terminals ($Q_{term} = Q_{perf}/N_{term}$); (*f*) blood viscosity ($h$ = 3.6 cP), corresponding to the high shear rate limit (Milnor, 1989; Lowe and Barbenel, 1988); and (*f*) flow resistance given by Poiseuille's law (Fung, 1984).

These conditions, jointly called "perfusion constraints," are supplemented by a bifurcation law

$$r_0^{\lambda} = r_1^{\lambda} + r_2^{\lambda} \quad (2)$$

which governs the shrinkage of segment radii across bifurcations. This form of power law (with different values for the exponent ) has been suggested by theoretical considerations (Rodbard, 1975; Sherman, 1981) as well as by morphometric measurements on coronary artery corrosion casts (Zamir, 1988). ($r_0$ is the parent and $r_1$ and $r_2$ are the larger and smaller daughter segments.)

The perfusion area, representing the piece of tissue to be supplied (100 g, see above), was chosen to be a flat circular disk of 5-cm radius, perfused from a point on the perimeter (Netter, 1983).

The locations of the distal ends of terminal segments are chosen using PRNS (Press et al., 1992; The Numerical Algorithms Group, 1993). Depending on the arbitrarily chosen initial value of the PRNS used, one obtains a specific instance of the model under otherwise unchanged conditions. Different instances correspond to the anatomical variability between individuals on top of a generally similar type of branching.

### *Trees Generated*

The target function parameter was varied between $\lambda = 0$ and $\lambda = 2$ in steps of 0.2, and two different trees were generated (from different PRNS seeds) for each value of $\lambda$. Additionally, two trees each were generated for $\lambda = 3$ and 4, yielding a total of 26 trees. For several choices of $\lambda$ there are intuitive geometrical interpretations: (*a*) $\lambda = 0$, optimization towards minimum sum of segment lengths (regardless of radii); (*b*) $\lambda = 1$, optimization towards minimum total surface of the tree; and (*c*) $\lambda = 2$, optimization towards minimum total volume (classic choice).

We note that for $\lambda = 1$ the target function (see Eq. 1) must be multiplied by $2\pi$ to actually yield the surface area. Since constant factors are irrelevant for minimization, we may with full right claim to minimize surface area when putting $\lambda = 1$ in Eq. 1. Likewise, a factor $\pi$ is necessary to arrive at the actual volume when inserting $\lambda = 2$ into Eq. 1. Intermediate (noninteger) values of $\lambda$ as well as the choices $\lambda = 3,4$ do not lend themselves to immediate geometrical interpretations. However, the fact that CCO works for arbitrary choices of $\lambda$, offers the unique opportunity to continuously vary the target function from length to volume and beyond and observe how the resulting structure responds. Since the constant in Eq. 1 neither influences the process nor the result of optimization it can be put equal to unity and need not be varied when optimizing for different values of $\lambda$.

### *Visual Inspection and Interpretation of CCO Trees for Different Target Functions*

In Fig. 1 we display visualizations of the trees generated for the integer values of $\lambda$ ($= 0, 1, 2, 3$). Even on visual inspection the impact of target function on structure is out of question.

Considering $\lambda = 0$ (Fig. 1 *A*), the target is to minimize the total sum of segment lengths, regardless of radii. In this case, the length of a small segment (small means small in radius) contributes to the sum with the same weight as the length of a large segment does. However, because there are many more small than large segments in a tree, the large ones make only a minor contribution to the total sum. Hence, to keep the total sum low ($\rightarrow$ minimization), it is more rewarding for CCO to keep the (majority of) small segments short rather than shorten the few large ones. The

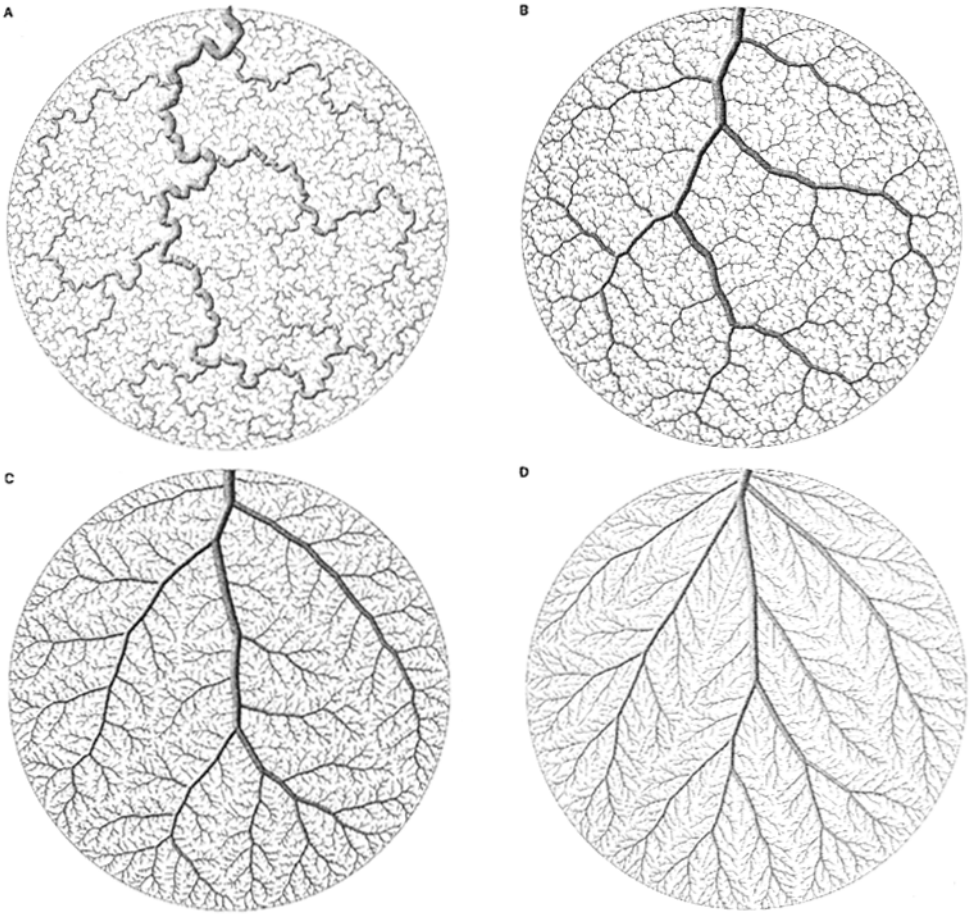


FIGURE 1. Visual impact of optimization target on vascular tree model structure. Trees of 4,000 terminals each were generated by constrained constructive optimization for several members of the target function family, Eq. 1. (*A*) $\lambda = 0$ (minimum sum of segment lengths). (*B*) $\lambda = 1$ (minimum total surface of tree). (*C*) $\lambda = 2$ (minimum total volume of tree). (*D*) $\lambda = 3$ (minimum hypervolume).

impact on structure is evident: large segments are allowed to form very curved vessels, each featuring frequent changes in direction. With $\lambda = 0$, there is almost no target function penalty for detours as long as they do not involve a large number of segments, which is not the case within the major branches.

Optimizing with $\lambda = 1$ (Fig. 1 *B*) means minimizing the total surface of the tree. In terms of sums and weights this can also be interpreted as follows: each term $l(i)$ in the target function Eq. 1 is multiplied by a factor $r(i)$, which may be considered as a weight proportional to segment radius. Hence, the length of a large segment enters with higher weight than the length of a small one, which intuitively corresponds to the relative importances. In terms of target function strategy, CCO now

has to be more restrictive in creating detours within major vessels. As a result, conspicuous detours are suppressed relative to $\lambda = 0$ (Fig. 1 *A*).

Turning to volume as minimization target ($\lambda = 2$; Fig. 1 *C*), this trend continues, and large vessels follow rather straight paths. In the target sum, each segment length is assigned a weight proportional to the cross-sectional area of the segment. Minimum volume is one of the generally accepted targets for optimization (Kamiya and Togawa, 1972), and we have exclusively used it in our previous studies on CCO (Schreiner and Buxbaum, 1993; Schreiner et al., 1994).

Setting $\lambda = 3$, i.e., minimizing the "hypervolume" of the tree (Fig. 1 *D*), means summing segment lengths with weights that depend more strongly on radius than the cross sectional area does. The result is striking: we obtain a totally straightened course for the large vessels. Moreover, large vessels now bifurcate very early, i.e., shortly downstream from the root. Branching angles become even more acute and the tree looks as if blood had to be conveyed to its deposition site as directly as possible.

As mentioned before, noninteger values of $\lambda$ do not have direct geometrical interpretations. However, since we do not know according to which target nature

TABLE I

*The Dual Role of Target Functions and Computed Quantities*

| $\lambda$ | **Target Function** | Sum of segment lengths $\sum_{i=1}^{N_{tot}} l(i)$ | Surface $2\pi \sum_{i=1}^{N_{tot}} l(i)\, r^1(i)$ | Volume $\pi \sum_{i=1}^{N_{tot}} l(i)\, r^2(i)$ | Surface × cross-section (hypervolume) $2\pi^2 \sum_{i=1}^{N_{tot}} l(i)\, r^3(i)$ | Volume × cross-section (hypervolume) $\pi^2 \sum_{i=1}^{N_{tot}} l(i)\, r^4(i)$ |
|---|---|---|---|---|---|---|
| | | *cm* | $cm^2$ | $cm^3$ | $cm^4$ | $cm^5$ |
| 0 | $\sum_{i=1}^{N_{tot}} l(i)$ | **591.1** | 87.8 | 2.2817 | 1.2793 | 0.072601 |
| 1 | $2\pi \sum_{i=1}^{N_{tot}} l(i)\, r^1(i)$ | 626.5 | **62.6** | 1.0081 | 0.40245 | 0.018109 |
| 2 | $\pi \sum_{i=1}^{N_{tot}} l(i)\, r^2(i)$ | 700.6 | 64.7 | **0.94515** | 0.34424 | 0.014242 |
| 3 | $2\pi^2 \sum_{i=1}^{N_{tot}} l(i)\, r^3(i)$ | 752.0 | 71.8 | 1.0124 | **0.33304** | 0.012309 |
| 4 | $\pi^2 \sum_{i=1}^{N_{tot}} l(i)\, r^4(i)$ | 764.1 | 90.1 | 1.3692 | 0.38222 | **0.010939** |

Arterial tree models were generated by CCO for a family of five target functions (column 2), being parameterized by the exponent $\lambda = 0, 1, 2, 3, 4$ (column 1), see Eq. 1. Each line in the table corresponds to one target function. For each tree generated, the target function's minimum is given in the bold-framed cells in the main diagonal. While one member of the target function family governs optimization (the "very" target function) the other members retreat into the roles of "computed quantities" which characterize the tree but do not influence its growth. Not that two trees were grown (from different random numbers) for each target function and mean values are given here. For one of the computed quantities, namely total volume, the spread within each pair of trees can be seen in Fig. 2. Also, Fig. 2 shows additional results for total volume in the range $0 < \lambda < 2$.

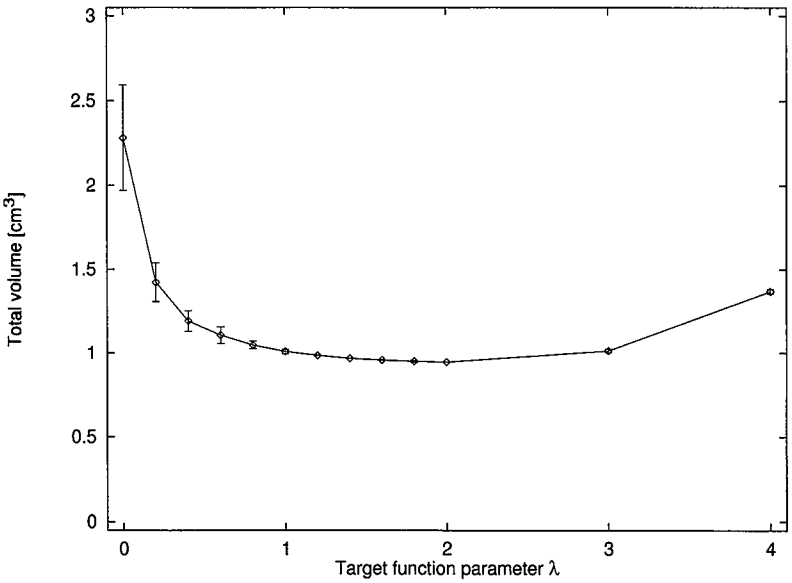


FIGURE 2. Impact of target on total volume. For each value of the target function parameter λ (x-axis), two trees were grown from different pseudo random number seeds. (y-axis) Total volume of tree model (cubic centimeters). The line joins mean values, bars denote standard deviations.

really optimized arterial trees, it is a strength of CCO that it can cope even with the formal extensions of geometrically interpretable targets.

*Degree of Optimization Achieved*

Considering a tree with $\lambda = 2$, the total volume plays the role of the optimization target. Of course, the sum of segment lengths and the total surface area may be computed as well, even though they have no influence on the optimization of the tree. Conversely, for $\lambda = 1$ the surface area assumes the role of the target while the sum of segment lengths and total volume may be computed for the resulting tree. A similar situation holds for $\lambda = 0$.

It is interesting to see how much difference it makes for each of these three quantities (sum of lengths, surface, volume) whether they guide or just accompany optimization, i.e., whether they are used as target function or not. Obviously each quantity must take on minimum value when being target itself, since it is the object of minimization. This is confirmed by the results shown in Table I, where column minima always occur at the main diagonal of the matrix. From its column minimum, each quantity increases steadily towards both larger and smaller values of λ. For the total volume, this dependence is shown in more detail in Fig. 2, including also noninteger values of λ.

For each computed quantity the degree of optimality achieved can be characterized by comparing its column minimum and maximum. For example, the sum of segment lengths increases from 591.1 (top of column) to 764.1 (bottom of col-

umn). In other words, the total length rises (i.e., becomes suboptimal) by a factor of 1.29 if we optimize for $\lambda = 4$ instead of $\lambda = 0$. This is really a surprisingly small increase if we consider the striking difference in visual appearance (see Fig. 1). It means that the sum of segment lengths by itself is not a sensitive parameter to discriminate differences in tree structure as shown in Fig. 1. The monotonous increase of the sum of segment lengths towards $\lambda = 4$ can be explained by the concomitant decrease of the relative weight of segment length within the target function.

The other global measures show a larger increase when being deprived of their role as optimization target. Surface rises by a factor of 1.44 for $\lambda = 4$ (compared to $\lambda = 1$) and volume by a factor of 2.41 for $\lambda = 0$ (compared to $\lambda = 2$). The hypervolumes ($\lambda = 3$ and 4) appear even more sensitive and increase by factors of 3.84 and 6.64, respectively, for $\lambda = 0$. Whereas in the first column of Table I the sum of segment lengths increases with $\lambda$ (from top to bottom), the computed quantity in the rightmost column (volume $\times$ cross-section) increases steadily as $\lambda$ decreases (bottom to top).

*Numerical Characterization of Structural Features*

In addition to various members of the family of target functions (Eq. 1), a number of other quantities can be constructed and calculated to describe structural features of an arterial model tree. Of course, we are primarily interested in quantities representing functional aspects relevant for blood transport capability.

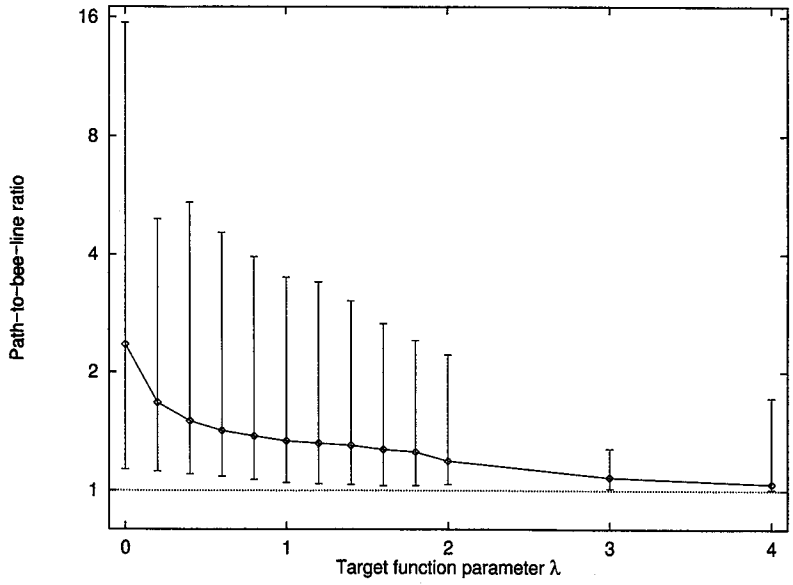


FIGURE 3. Impact of target on blood transport path length. (x-axis) Optimization target function parameter $\lambda$. (y-axis) Path-to-bee-line ratio, averaged over all terminal segments of a tree: $\langle L_{path}/L_{beeline}\rangle_{\text{all terminals}}$. The line joins the mean values, bars denote minima and maxima.

*Path Length for Blood Transport*

From the inlet of the model tree towards a given terminal segment blood has to traverse a certain sequence of segments, called "path." Its length $L_{path}$ is the sum of the individual segment lengths that is obviously always longer than a straight line (the bee-line with length $L_{bee\text{-}line}$) between the proximal end of the root and the distal end of the respective terminal segment. The presence of detours lengthens the path as compared to the bee-line, which can be expressed quantitatively by considering the ratio $L_{path}/L_{bee\text{-}line}$ which is a dimensionless quantity. Averaging this ratio over all terminal segments we obtain the path-to-bee-line-ratio

$$R_L = \langle L_{path}/L_{bee-line} \rangle_{\text{all terminals}} \tag{3}$$

which is a measure for the relative increase in path length because of detours within a given model tree. Fig. 3 shows the dependence of $R_L$ on the target function parameter $\lambda$, and quantitatively confirms what has already been qualitatively described: for $\lambda = 0$ the path length from the root to a terminal is on the average 2.3 times longer than the bee-line, which is a consequence of numerous severe detours through the strongly curved vessels, see Fig. 1 *A*. The extent of detours varies between regions of the tree as indicated by the HI-LO bars. As $\lambda$ increases, the extent of detours decreases steadily towards a surprisingly low value of 1.08 for $\lambda = 3$. This corresponds to a markedly streamlined course of the vessels as seen in Fig. 1, *D*, where the average path through the vasculature is only 8% longer than a straight line! For $\lambda = 4$, $R_L$ even decreases to 1.04.

Within each tree the distribution of path-to-bee-line ratios is skewed towards lower values. For each terminal segment, the path-to-bee-line ratio must be larger than 1, and in fact very straight paths occur even in trees with $\lambda > 1$, as shown by the LO-bars in Fig. 3. The longest detours are observed for $\lambda = 0$ (indicated by the HI-bars in Fig. 3), reaching up to 16 times the length of a straight line, and decreased continuously for the more streamlined structures with $\lambda > 0$.

*Pressure Profile*

At the inlet, our model tree is perfused by a pressure $p_{perf}$. According to Poiseuille's law, pressure decreases along each segment and, when tracing a path distally, we reach a uniform, preset terminal pressure, $p_{term}$, at the respective terminal. In between we may compute the pressure profile that is considered to be a key descriptor of vascular tree functionality and results from several determinants.

Above all, it is the bifurcation law that determines the area expansion ratio (van Bavel and Spaan, 1992) via the shrinkage of radii and thus has the largest effect on the pressure profile. This has been demonstrated previously in the framework of CCO models (Schreiner and Buxbaum, 1993), when we found that the choice $\gamma = 2.55$ seemed more adequate than the classical value of 3.0. Incidentally, $\gamma = 2.55$ would be necessary to minimize wave reflections at bifurcations (Arts, Kruger, van Gerven, Lambregts, and Reneman, 1979) whereas $\gamma = 3.00$ is a condition for uniform shear stress and was also confirmed experimentally on corrosion casts (Zamir and Chee, 1987; Zamir, 1988).

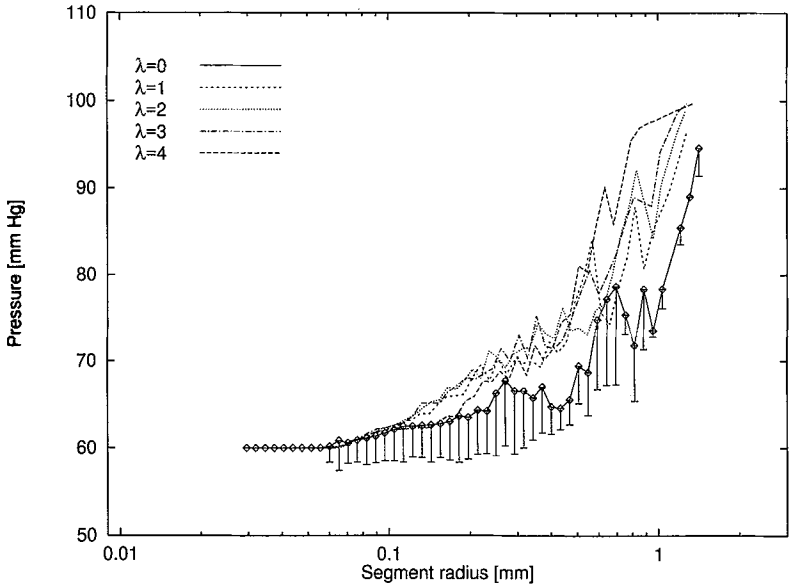


FIGURE 4. Impact of target on pressure profile for bifurcation constraint $\gamma = 3$. (x-axis) Segment radius (millimeters). (y-axis) Pressure [mmHg] at distal end of segment. The lines join mean values over segment classes equidistant on a log scale, for the profile $\lambda = 0$ (i.e., sum of segment length is target) bars denote standard deviations. Each line corresponds to a whole tree with the optimization parameter given in the legend.

Second, a different geometry may also influence the pressure profile. After all we can expect that it is not irrelevant along which path (curved or straight) one reaches a terminal. Thus, we also investigated the impact of changing targets on the pressure profiles in our CCO models.

Segment radii were binned into equidistant classes of radius on a logarithmic scale, and mean pressures (at the distal ends of the segment) computed. One model tree each for $\lambda = 0$, 1, 2, 3, and 4 was examined, yielding results shown in Fig. 4. For the target $\lambda = 0$ pressure first decreases rapidly, indicating that a major part of resistance is located in the large segments. Conversely, the very straight structure with $\lambda = 4$ shows very little resistance in the large segments and has its major decrease of pressure (slope) in the medium sized segments. The other profiles lie somewhere in between and, despite a distinct effect of target, none of the profiles looks realistic and satisfying, since pressure profiles (in the vasodilated state) are expected to appear as straight lines in a semi-logarithmic plot (van Beek, Roger, and Bassingthwaighte, 1989).

Therefore, we performed five additional simulations with a different bifurcation constraint, namely $\gamma = 2.55$, and $\lambda = 0$, 1, 2, 3, and 4, resulting in the pressure profiles shown in Fig. 5. Indeed, for $\lambda = 1$, 2, and 3 the plots now appear to be more consistent with straight lines.

Our major conclusion, which we like to anticipate here in the result section, is that $\lambda = 0$ and $\lambda = 4$ can be ruled out and the family of realistic targets thus re-

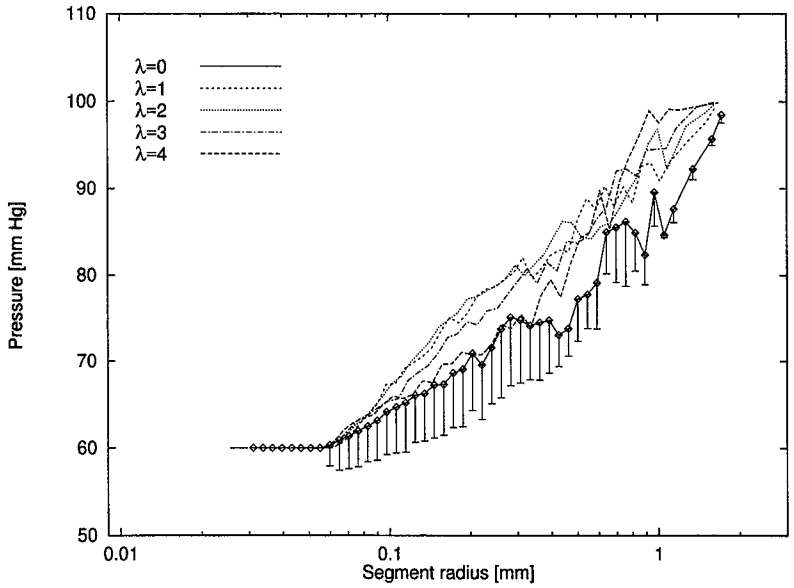


FIGURE 5. Impact of target on pressure profile for bifurcation constraint $\gamma = 2.55$. Notation like Fig. 4. Profiles for $\lambda = 1$, 2, and 3 almost lie on straight lines, as expected for vasodilated beds (van Beek et al. 1989).

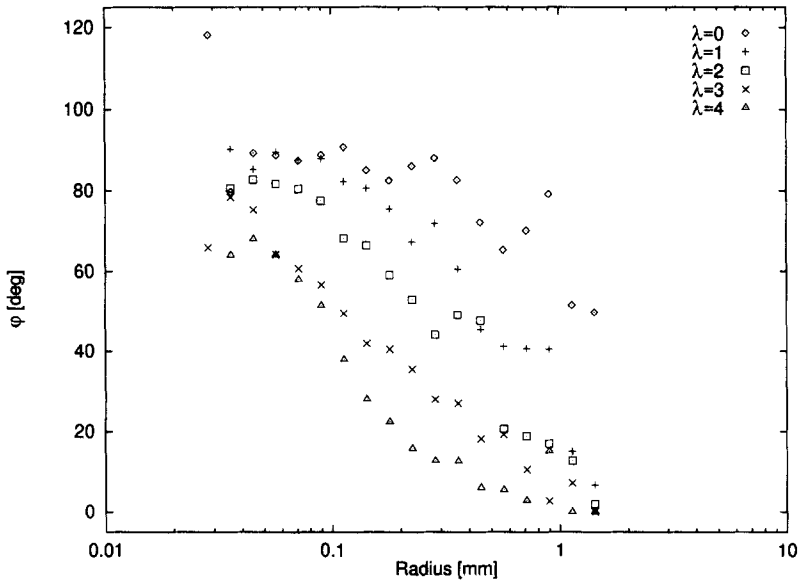


FIGURE 6. Impact of target on segment orientation. Each symbol refers to a separate tree and target ($\lambda$), see the legend. (x-axis) Segment radius (millimeters). (y-axis) Angle (degree) between segment orientation and the bee-line connecting the tree's inlet with distal end of the respective segment. Symbols give mean angles over segment classes equidistant on a log scale for radius.

duces to $1 \leq \lambda \leq 3$ as far as the reproduction of a realistic pressure profile is concerned. However, even in these cases a different bifurcation constraint of $\gamma < 3$ is mandatory. As a consequence of these findings we shall comment on a few aspects of the dual relation between constraints, targets, and computed quantities in the frame of CCO in the discussion section.

### *Segment Orientation*

Branching angles characterize the difference in orientation between successive segments (parent, daughters). In our previous study (Schreiner et al., 1994) we have demonstrated that for the target $\lambda = 2$ the dependence of branching angles on the diameter ratio satisfactorily reproduces measurements from corrosion casts (Zamir and Chee, 1986). Preliminary evaluations revealed that the distribution of branching angles can only discriminate between $\lambda = 0$, 1, and 2, but not between $\lambda = 2$, 3, and 4, although visually the difference is obvious. Excessive streamlining ($\lambda > 2$) seems to have no additional impact on the angles between parent and daughters.

We therefore constructed the segment orientation as a new morphometric descriptor of tree structure. Considering a particular segment we compute the angle between the segment's direction and the straight line between the tree's inlet and the distal end of that segment (bee-line for arbitrary segments). This angle characterizes the deviation between the direction in which blood is conveyed within the segment and the direction in which blood would be conveyed directly (bee-line). When inspecting the streamlined structures in Fig. 1, one can expect especially the large segments to closely parallel the corresponding bee-lines. Hence, in Fig. 6 we averaged segment-to-bee-line-angles ($\varphi$) over classes of radii and found (as expected) that: (*a*) angles are generally lower for large targets (i.e., large values of $\lambda$). (*b*) for all targets the orientation of large segments is closer to the bee-line's orientation than it is for small radii; and (*c*) for $\lambda = 0$ angles decrease slowly with increasing radius (the zig-zag course is still present even in large arteries) whereas for $\lambda = 4$ large angles are found in the smallest segments only.

In conclusion, the angle between segment and bee-line discriminates structures over the whole range of targets $0 \leq \lambda \leq 4$ and is an indicator particularly for the degree of stream-lining. In contrast, branching angles only discern the diminishing zigzag course of vessels when $\lambda$ increases from 0 to 2.

## DISCUSSION

### *Aims, Findings, and Concepts*

The aim of the present paper was to investigate if and how the model tree structure reacts on changing the target function used in Constrained Constructive Optimization. To these ends, we extended the method of CCO for the first time to a parameterized class of target functions, of which the previously used total intravasal volume is a representative.

The effect of changing the target was both visually displayed (Fig. 1) and quantitatively characterized. In a first step towards quantification of structure, we computed quantities intrinsically related to the tree as a whole, such as total volume, to-

tal surface, and the sum of segment lengths. Second, we considered quantities that primarily have a local meaning, such as the path-to-bee-line ratio and relative segment orientation. Computing averages of these quantities over a whole tree also provides suitable global descriptors of structure. In particular, the following results were obtained: (*a*) global characteristics generally react in a smooth rather than in a discontinuous way on gradual changes of the target function via its parameter; (*b*) sum of segment lengths, total surface, volume, and hypervolumes are lowest if and only if they are used as target functions (these quantities may be up to six times larger if the tree is optimized for a different target); (*c*) different computed characteristics, such as path lengths and relative segment orientation, can be used to illuminate different aspects of the same phenomenon (zig-zag vs straight course of vessels); (*d*) it is possible to understand why an increase in $\lambda$ changes structure from twisted to straight (see the discussion on the increasing weight of radii) (in this sense, the intrinsic mechanism of CCO has been made transparent regarding the relation between our family of target functions and structural aspects of the resulting model trees); (*e*) in most cases the path-to-bee-line-ratio came out surprisingly low, which means that a more or less direct access to blood deposition sites was achieved despite the full implementation of all constraints; (*f*) the pressure profile seems to depend more strongly on $\gamma$ than on $\lambda$; (*g*) segment orientation with reference to the respective bee-line was found to discriminate satisfactorily between target functions, even for $\lambda \geq 2$, were conventional branching angles cannot discriminate any more; and (*h*) as a by-product not mentioned before, we found that the number of bifurcation levels decreases drastically as $\lambda$ increases. While the trees with $\lambda = 0$ had $\sim$160 bifurcation levels, we found $\sim$105, 115, 100, and 70 bifurcation levels for $\lambda = 1$, 2, 3, and 4, respectively. Inspecting Fig. 1 *D*, the reason is clear: in the straight tree, large branches bifurcate early, fairly symmetrically and in rapid succession. Because each (approximately) symmetric bifurcation roughly doubles the number of distal terminals that can be supplied, fewer bifurcation levels suffice to split into a given number of terminals. Conversely, highly asymmetric offsprings from large segments (Fig. 1 *A*) increase the bifurcation levels of all distal segments while supplying only a very limited number of terminals themselves.

### *Reviewing Specific Aspects of CCO*

The method of CCO is applicable to various types of perfusion areas in two or three dimensions. In the present work we choose a circle as the most simple case, since it already suffices to demonstrate the key issue, namely the impact of optimization target selection. A realistically shaped two-dimensional perfusion area has previously been illustrated (Schreiner, 1993) and a concept for possible generalizations to three dimensions has been outlined (Schreiner et al., 1994).

The previous section on pressure profiles is a vivid example for the simultaneous dependence of CCO models on both constraints and optimization targets.

Thus, to successfully model nature, we have to make sensible assumptions about targets and constraints. This demonstrates both the versatility and the pitfalls of CCO. An unfortunate choice of constraints may preclude satisfying results even under proper optimization targets and vice versa. For example, imposing an unrealis-

tic constraint (i.e., $\gamma = 1$) would still yield literally optimized trees (e.g., for minimum volume), but daughter segments would in this scenario systematically be too thin in relation to their parents, thus leading to an unrealistic pressure profile. This example also illustrates that each specific constraint usually exerts a specific influence on one (or several) functional characteristics, and we therefore need to investigate several characteristics to comprehensively evaluate the performance of a given CCO setup (constraints and target).

There is a dual relation (interchangeability) between constraints and target. For example, the bifurcation constraint has originally been chosen as $\gamma = 3$ to allow for uniform distribution of shear stress (Rodbard, 1975; Sherman, 1981) that could also be selected as a target for optimization. In the present form of CCO however, it enters as boundary condition. In fact, to some extent we have the choice what to impose as constraint and what to optimize under that constraint. Other settings of CCO could be thought of, in which constraints and targets interchange roles. Similar arguments apply to other possible interchanges within constraints and resulting quantities. For example in the present setup, equal flows and equal pressures at all terminals are the constraints, and (unequal) radii of terminal segments result therefrom. These constraints aim at supplying microcirculatory black boxes of similar size with equal flows (at equal pressures). Alternatively one could require equality of terminal radii. Then we would have to sacrifice the equality of either terminal flows or else of terminal pressures.

In this work we have implicitly assumed that the very same set of target and constraints applies all over the tree. One may also think of spatially changing, or blended targets which, e.g., optimize large and small vessels according to different rules. This could lead to even more realistic structures, since large and small vessels have different physiologic tasks to perform (transport of blood vs delivery of nutrients). Up to now however, due to the lack of a quantitative basis, any such approach would be highly speculative.

In summary, a whole variety of different modes of CCO can be thought of, and the evaluation of their relative merits is a challenging task for coming studies. In the present work, we have investigated only one special representative of CCO for one parameterized class of target functions.

The authors are grateful for valuable hints from an unknown referee, which encouraged us to develop and investigate the concept of relative segment orientation.

This work was supported by the Ludwig Boltzmann Institut für Herzchirurgische Forschung and the Bundesministerium für Wissenschaft und Forschung, grant 49.820/4-24/92.

*Original version received 19 January 1995 and accepted version received 23 June 1995.*

## REFERENCES

Arts, T., R. T. I. Kruger, W. van Gerven, J. A. C. Lambregts, and R. S. Reneman. 1979. Propagation velocity and reflection of pressure waves in the canine coronary artery. *American Journal of Physiology.* 237:469–474.

Bruinsma, P., T. Arts, J. Dankelman, and J. A. E. Spaan. 1988. Model of the coronary circulation

based on pressure dependence of coronary resistance and compliance. *Basic Research in Cardiology.* 83:510–524.

Chilian, W. M., S. M. Layne, E. C. Klausner, C. L. Eastham, and M. L. Marcus. 1989. Redistribution of microvascular resistance produced by dipyridamole. *American Journal of Physiology.* 256:H383–H390.

Cohn, D. L. 1955. Optimal systems: II. The cardiovascular system. *Bulletin of Mathematical Biophysics.* 17:219–227.

Dawant, B., M. Levin, and A. S. Popel. 1985. Effect of dispersion of vessel diameters and lengths in stochastic networks I. Modeling of microcirculatory flow. *Microvascular Research.* 31:203–222.

Fung, Y. C. 1984. Biodynamics: Circulation. Springer-Verlag, NY.

Kamiya, A., and T. Togawa. 1972. Optimal branching structure of the vascular tree. *Bulletin of Mathematical Biophysics.* 34:431–438.

Lefevre, J. 1982. Teleonomical representation of the pulmonary arterial bed of the dog by a fractal tree. *In* Cardiovascular System Dynamics: Models and Measurements. T. Kenner, R. Busse, and H. Hinghofer-Szalkay, editors. Plenum Publishing Corp., NY. 137–146.

Lefevre, J. 1983. Teleonomical optimization of a fractal model of the pulmonary arterial bed. *Journal of Theoretical Biology.* 102:225–248.

Levin, M., B. Dawant, and A. S. Popel. 1986. Effect of dispersion of vessel diameters and lengths in stochastic networks II. Modeling of microvascular hematocrit distribution. *Microvascular Research.* 31:223–234.

Lowe, G. D. O., and J. C. Barbenel. 1988. Plasma and blood viscosity. *In* Clinical Blood Rheology. G. D. O. Lowe, editor. CRC Press, Boca Raton, FL. 11–44.

Marzilli, M., S. Goldstein, H. N. Sabbah, T. Lee, and P. D. Stein. 1979. Modulating effect of regional myocardial performance on local myocardial perfusion in the dog. *Circulation Research.* 45:634–640.

Milnor, W. R. 1989. Hemodynamics. Williams and Wilkins, Baltimore, MD.

Netter, F. H. 1983. Heart: The Ciba Collection of Medical Illustrations. Thieme-Verlag, NY.

Pelosi, G., G. Saviozzi, M. G. Trivella, and A. L'Abbate. 1987. Small artery occlusion: a theoretical approach to the definition of coronary architecture and resistance by a branching tree model. *Microvascular Research.* 34:318–335.

Press, W. H., S. A. Teukolsky, W. T. Vetterling, and B. P. Flannery. 1992. Numerical recipes in FORTRAN, the art of scientific computing. Cambridge University Press, Cambridge, UK.

Rodbard, S. 1975. Vascular Caliber. *Cardiology.* 60:4–49.

Rooz, E., T. F. Wiesner, and R. M. Nerem. 1985. Epicardial coronary blood flow including the presence of stenosis and aorto-coronary bypasses. I. Model and numerical method. *ASME Journal of Biomechanical Engineering.* 107:361–367.

Schreiner, W. 1993. Computer generation of complex arterial tree models. *Journal of Biomedical Engineering.* 15:148–150.

Schreiner, W., and P. F. Buxbaum. 1993. Computer-optimization of vascular trees. *IEEE Transactions on Biomedical Engineering.* 40:482–491.

Schreiner, W., M. Neumann, F. Neumann, S. M. Roedler, A. End, P. F. Buxbaum, M. R. Müller, and P. Spieckermann. 1994. The branching angles in computer-generated optimized models of arterial trees. *Journal of General Physiology.* 103:975–989.

Sherman, T. F. 1981. On connecting large vessels to small: the meaning of MURRAY's law. *Journal of General Physiology.* 78:431–453.

Sun, Y., and H. Gewirtz. 1988. Estimation of intramyocardial pressure and coronary blood flow distribution. *American Journal of Physiology.* 255:H664–H672.

The Numerical Algorithms Group. 1993. NAG FORTRAN Library Manual, Mark 16. The Numerical Algorithms Group, Oxford, UK.

Thompson, D. W. 1952. On growth and form. Volume II. University Press, Cambridge, UK. 948–957.

van Bavel, E., and J. A. E. Spaan. 1992. Branching patterns in the porcine coronary arterial tree estimation of flow heterogeneity. *Circulation Research.* 71:1200–1212.

van Beek, J. H. G. M., S. A. Roger, and J. B. Bassingthwaighte. 1989. Regional myocardial flow heterogeneity explained with fractal networks. *American Journal of Physiology.* 257:H1670–H1680.

West, B. J., and A. L. Goldberger. 1987. Physiology in fractal dimensions. *American Scientist.* 75:354–364.

Zamir, M. 1976. Optimality principles in arterial branching. *Journal of Theoretical Biology.* 62:227–251.

Zamir, M., and D. C. Bigelow. 1984. Cost of deparature from optimality in arterial branching. *Journal of Theoretical Biology.* 109:401–409.

Zamir, M., and H. Chee. 1986. Branching characteristics of human coronary arteries. *Canadian Journal of Physiology and Pharmacology.* 64:661–668.

Zamir, M., and H. Chee. 1987. Segment analysis of human coronary arteries. *Blood Vessels.* 24:76–84.

Zamir, M. 1988. Distributing and delivering vessels of the human heart. *Journal of General Physiology.* 91:725–735.

Zamir, M., and P. Sinclair. 1988. Roots and calibers of the human coronary arteries. *American Journal of Anatomy.* 183:226–234.